Available online at www.sciencedirect.com
ScienceDirect
Trans. Nonferrous Met. Soc. China 34(2024) 1037−1048
Transactions of Nonferrous Metals Society of China
www.tnmsc.cn

Purification of metallurgical-grade crude tellurium based on viscous distillation and gas-phase separation

Da-xin HUANG[1,2,3], Wen-long JIANG[1,2,3], Bao-qiang XU[1,2,3], Guo-zheng ZHA[1,2,3], Bin YANG[1,2,3]

1. National Engineering Research Center of Vacuum Metallurgy, Kunming University of Science and Technology, Kunming 650093, China;
2. State Key Laboratory of Complex Non-ferrous Metal Resources Clean Utilization, Kunming University of Science and Technology, Kunming 650093, China;
3. Faculty of Metallurgical and Energy Engineering, Kunming University of Science and Technology, Kunming 650093, China

Received 5 October 2022; accepted 10 April 2023

Abstract: A method for preparing high-purity tellurium based on viscous distillation and gas-phase separation was developed. By adjusting the condenser structure and condensing temperature to achieve viscous distillation, the dominant condensation zone for tellurium was controlled; hence, poorly volatile substances remained in the crucible, while selenium was separated from tellurium in the gas phase to achieve the purification of metallurgical-grade crude tellurium. Specifically, the saturated vapor pressure, mean free path of tellurium, impurity distribution, and morphologies of the condensate at different locations were investigated in detail. The results for a 500 g upscaled experiment showed that the direct yield of Te was 83.40%, the purity of Te reached higher than 99.9996 wt.% and the selenium content in the dominant condensation zone was reduced to 2.76×10^{-4} wt.% under the optimal experimental conditions of 5 Pa, 773 K and 90 min.

Key words: high-purity tellurium; selenium removal; refinement; mean free path; dominant condensation zone

1 Introduction

Tellurium is a scattered element and is widely used in the semiconductor, chemical, metallurgy, medicine, and photovoltaic fields [1,2]. In particular, with the increasing demand for tellurium in emerging fields such as solar energy and semiconductors, especially CdTe photoelectric glass and Bi_2Te_3 thermoelectric materials, high-purity tellurium has become one of the key materials supporting high-tech development and new product development [3,4]. The performance of the product depends largely on the purity of the initial materials [5,6]. However, the tellurium extracted from anode slime is generally metallurgical grade (99.0%−99.9%), which does not meet the requirements for new materials. Achieving green and efficient purification of crude tellurium to enhance its added value has become an urgent issue for tellurium and copper producers worldwide.

Some chemical methods are available for tellurium refining, including oxidation–reduction, selective precipitation and electrowinning [7,8]. These methods use the differences in chemical properties for tellurium and the impurity elements to generate intermediate compounds by adding chemical reagents and then separating impurities [9].

Corresponding author: Wen-long JIANG, Tel: +86-15987187472, E-mail: wenlong_jiang@kust.edu.cn;
Bin YANG, Tel: +86-13888113129, E-mail: kgyb2013@kust.edu.cn
DOI: 10.1016/S1003-6326(23)66452-0

Although satisfactory purity can be obtained, these technologies often require repeated oxidations and reductions of the elements during the purification process, often involve toxic and hazardous substances and are accompanied by considerable production safety and waste disposal issues [10]. Physical methods for purifying tellurium based on differences in the physical properties for the impurity element and tellurium mainly include zone smelting and vacuum distillation [11]. No reagents are added during the zone smelting process, so no impurities are introduced [12]. However, this process is very time-consuming and has a low production rate, so it is only suitable for producing small amounts of ultrahigh-purity metal [13,14]. In contrast, interest in vacuum distillation technology is growing, and this is carried out in a closed system under atmospheric pressure and is characterized by low energy consumption, high efficiency, low pollution and eco-friendliness [15]. It has been widely used in the fields of alloy separation [16,17], sustainable clean recycling of secondary resources [18], preparation of materials and high-purity metals [19], and remediation of hazardous waste [20,21].

Some studies have reported that vacuum distillation purifies crude tellurium efficiently. PRASAD et al [22] achieved the purification of tellurium to 5N5. ALI et al [23] reported that Te with 5N5 purity can be prepared with multiple distillations, and the relationship among the Te evaporation rate, time and effective separation coefficient was investigated by ZAIOUR et al [12]. Tellurium resources, either copper anode slime or its minerals, usually contain considerable amounts of selenium, so selenium is one of the most common impurities in crude tellurium [24]. Unfortunately, the separation of selenium and tellurium by vacuum distillation is inefficient due to the low separation coefficients of selenium and tellurium and azeotrope formation in the selenium and tellurium binary system [25−27]. Therefore, efficient separation of selenium from the tellurium is the bottleneck limiting vacuum distillation and purification of tellurium.

To address the problem of selenium and tellurium separation during vacuum distillation, viscous distillation and gas-phase separation (VDGS) were used in this study to purify crude tellurium. The saturated vapor pressure, mean free path, impurity distributions, condensate morphologies at different locations, and the results of a 500 g upscaled experiment were investigated in detail. This work lays a foundation for the development of new technology for clean and efficient purification of crude tellurium and provides a method for separating substances with similar physical properties.

2 Experimental

2.1 Materials

The initial material was produced at a copper electrolytic refining company in Yunnan Province, China. The results of inductively coupled plasma–mass spectrometry (ICP−MS) analysis for 15 impurity elements are shown in Table 1, which indicates that the contents of Na, Si, Cu, Pb, Se, Fe and other elements are relatively high.

2.2 Theoretical analysis of saturated vapor pressure

The solid and liquid forms of any substance have the tendency to volatilize into a gaseous form and vice versa [28]. The pressure of the vapor in equilibrium with the solid or liquid under closed conditions is called the saturated vapor pressure (p*). It is generally believed that materials with higher vapor pressures have greater volatility [29]. The saturated vapor pressure p* is often nonlinearly related to temperature (T), and the relationship can be expressed by the derivative of the Clausius–Clapeyron equation as follows [30]:

$$\lg(kp^*)=AT^{-1}+B\lg T+CT+D \quad (1)$$

where k is a constant equal to 1×10^3, and A, B, C, and D are evaporation constants obtained from the literature [31].

The saturated vapor pressure can be calculated with Eq. (1). Figure 1(a) shows the saturated vapor pressures for Te and the 15 main impurities at 623, 673, 723, 773 and 823 K. The saturated vapor pressure of Se is higher than that of Te, while the Zn saturated vapor pressure is similar to that of Te, meaning that Se and Zn will theoretically evaporate with Te. Other elements with low saturated vapor pressures are easily removed as residues. With increasing distillation temperature, the saturated vapor pressures of the elements increase, and high

Table 1 Analytical results of ICP−MS (wt.%)

Element	Initial material	Residue	Level 1	Level 2	Levels 3 and 4	Levels 5 and 6
Na	0.1667	0.3488	1.79×10^{-4}	9.20×10^{-5}	9.00×10^{-5}	9.70×10^{-5}
Mg	2.10×10^{-5}	1.30×10^{-4}	1.90×10^{-5}	3.70×10^{-5}	3.60×10^{-5}	2.00×10^{-5}
Al	1.01×10^{-3}	4.03×10^{-3}	2.90×10^{-5}	–	–	–
Si	1.39×10^{-3}	3.12×10^{-3}	–	–	–	–
Ni	8.30×10^{-4}	3.90×10^{-3}	2.40×10^{-5}	1.10×10^{-5}	–	1.00×10^{-5}
Cu	3.34×10^{-3}	1.10×10^{-2}	1.43×10^{-4}	4.60×10^{-5}	4.50×10^{-5}	4.60×10^{-5}
Zn	1.50×10^{-4}	4.10×10^{-4}	1.23×10^{-4}	1.10×10^{-5}	1.30×10^{-5}	1.50×10^{-5}
Se	8.70×10^{-4}	4.20×10^{-4}	2.59×10^{-4}	3.80×10^{-4}	4.00×10^{-4}	2.47×10^{-3}
Pb	4.93×10^{-3}	2.46×10^{-2}	2.00×10^{-5}	8.00×10^{-5}	8.10×10^{-5}	1.32×10^{-4}
Fe	6.58×10^{-3}	3.38×10^{-2}	–	–	–	–
Bi	2.40×10^{-5}	6.80×10^{-5}	–	–	–	–
Sn	7.70×10^{-5}	2.30×10^{-4}	–	–	–	–
Ag	6.10×10^{-4}	1.95×10^{-3}	–	–	–	–
Cr	3.81×10^{-3}	1.05×10^{-2}	–	–	–	–
Mn	4.70×10^{-4}	3.18×10^{-3}	–	3.70×10^{-5}	3.10×10^{-5}	4.80×10^{-5}
Total impurity	0.190812	0.446138	7.96×10^{-4}	6.94×10^{-4}	6.96×10^{-4}	2.838×10^{-3}
Te	99.809188	99.553862	99.999204	99.999306	99.999304	99.997162

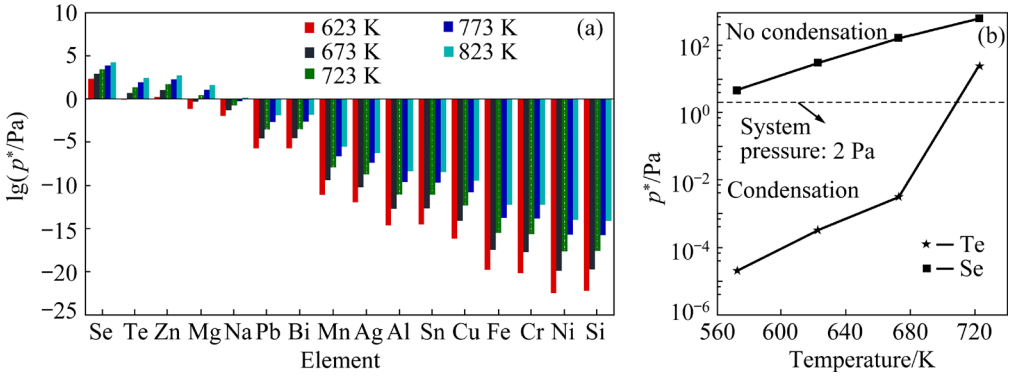

Fig. 1 Saturated vapor pressure versus temperature for tellurium and impurity elements (a) and condensing temperature as function of saturated vapor pressure for tellurium and selenium (b)

temperatures are not useful for separating the elements. Hence, by controlling certain conditions, nonvolatile substances can be left in the crucible. In addition, as shown in Fig. 1, tellurium preferentially condenses with the decrease in temperature in the gas phase, while selenium condenses later, which can achieve the purpose of separating selenium and tellurium in the gas phase.

2.3 Theoretical analysis of mean free path

The mean free path (λ) is an important factor affecting the movements of vapor molecules, and this determines the nature of the distillation process, i.e., either viscous distillation ($\lambda < L$) or molecular distillation ($\lambda > L$), where L is the distance between the melt surface and the condenser. When the vapor of an element is monoatomic, the effects of temperature and pressure on the mean free path can be described as follows [22]:

$$\lambda=3.11\times10^{-18}T/(d^2p) \quad (2)$$

where p is the system pressure, 2 Pa; d is the diameter of the vapor molecule, 272×10^{-10} cm for Te.

At 623, 673, 723, 773 and 823 K, the λ values for Te were calculated as 1.31, 1.41, 1.52, 1.62 and

1.73 cm, respectively. Hence, by changing the condenser structure ($\lambda < L$) and condensing temperature, viscous distillation can be achieved. Thus, the diffusion of tellurium in the gas phase is inhibited, as much tellurium as possible is condensed in the high-temperature condensation zone, and the dominant condensation zone of tellurium is controlled; selenium does not condense in this zone because of the lower condensing temperature and is separated from tellurium in the gas phase.

2.4 Experimental procedure

Vacuum distillation equipment (Fig. 2(a)) mainly consisting of an automatic control system, a vacuum system, and a cooling system was used in the purification experiments. The distillation chamber of the stainless-steel furnace (Fig. 2(b)) was composed of a thermocouple, a refractory device, a heater, a quartz crucible measuring 3 cm in diameter and 8 cm in height and a condenser measuring 10 cm in diameter and 12.5 cm in total height. In the experimental preparation stage, the evaporation crucible and condenser made of quartz were cleaned with alcohol and deionized water, and the furnace was evacuated for approximately 3 h at 873 K to remove the moisture. Then, 30 g of the initial input material was added to the quartz crucible for the experiment. The migration and distribution of the impurity elements and tellurium were studied carefully at different distillation temperatures and time. At the end of distillation, when the temperature in the chamber was dropped to room temperature, each zone of the condenser was removed for weighing, sampling and analysis. The vacuum pump continued running during the cooling process, ensuring that the system was always under vacuum, thus preventing gas leakage and metal oxidation.

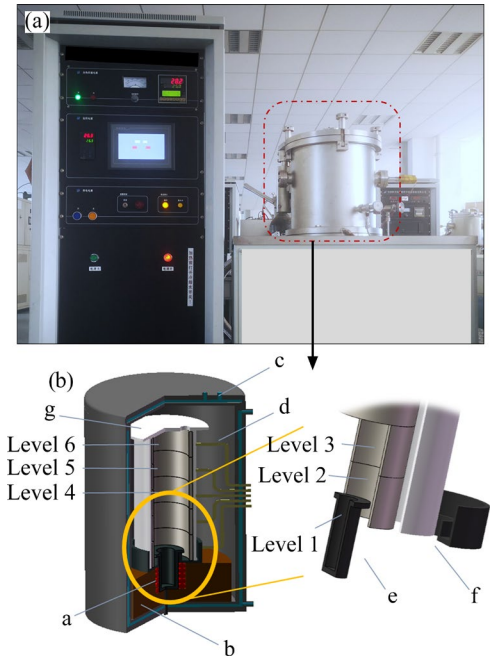

Fig. 2 Photograph (a) and structural diagram (b) of vacuum furnace: a−Heater; b−Insulation materials; c−Circulating condensate; d−Thermocouple; e−Crucible; f−Condenser; g−Condenser cap

Based on the small-scale experiment, a 500 g upscaled experiment was carried out to investigate the effects of different gasification temperatures and gasification time on the tellurium purity, evaporation rate and impurity removal rate. The results provide a foundation for the industrial application of the VDGS method.

2.5 Characterization

The contents of the 15 main impurities were determined with ICP–MS (7700x, Agilent, America) according to the Standards for the Nonferrous Metals Industry of PRC (YS/T 1013—2014) issued by the Ministry of Industry and Information Technology, China. Then, the purity of the distilled tellurium was calculated as 100% minus the total impurities. Samples for analysis were taken from different condenser locations by random selection from five places at the same level and mixed to obtain an average impurity result. The phases of the obtained samples were determined by X-ray diffraction (XRD) with a scan speed of 0.02 (°)/s over 2θ range and a Rigaku/D-Mac−3c X-ray diffractometer using Cu K_α radiation. The surface morphology of the crude tellurium was analyzed by scanning electron microscopy (SEM, JSM−7200F, JEOL, Japan) at an accelerating voltage of 10 kV. The surface morphologies and elemental distributions of the impurities in the samples were analyzed with an electron probe microanalyzer (EPMA, JXA8230, JEOL, Japan) operated with an accelerating voltage of 15 kV and a beam current of 2×10^{-9} A.

The evaporation rate (R_e) is defined as follows:

$$R_e=(m_0-m_r)/m_0\times100\% \quad (3)$$

where m_r is the mass of the residue and m_0 is the mass of the initial material.

The mass distribution rate (R_m) for each level

of VDGS can be described as follows:

$$R_m=m_i/m_0\times100\% \quad (4)$$

where m_i is the mass of the condensate in Level i.

The removal rate (R_r) of an element is defined as follows:

$$R_r=(1-w_{al}/w_{a0})\times100\% \quad (5)$$

where w_{al} is the content of the element in the condensate of the low-temperature heating zone (LTHZ) and w_{a0} is the content of the element in the initial material.

The direct yield of Te (Y_d) is defined as follows:

$$Y_d=(m_l w_{il})/(m_0 w_{i0})\times100\% \quad (6)$$

where m_l is the mass of the condensate in the LTHZ, w_{il} is the content of Te in the condensate of the LTHZ, and w_{i0} is the content of Te in the initial material.

3 Results and discussion

3.1 Results of VDGS

3.1.1 Migration and distribution characteristics of tellurium and impurity elements

First, the migration and distribution of tellurium and the impurity elements were studied under the conditions of 723 K, 120 min and 2 Pa. The temperature and condensate mass of each condensing zone are shown in Fig. 3. The evaporation rate reached 66.27%; more than 58% of the tellurium was condensed in the high-temperature condensation zone at 603.30 K (Fig. 2(b), Level 1), which was the dominant condensation zone

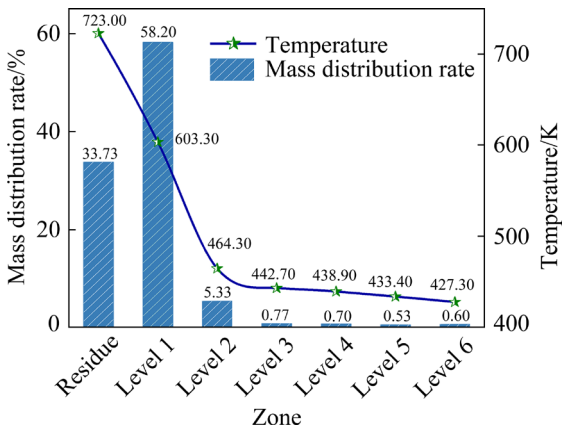

Fig. 3 Mass distribution rate at end of VDGS and temperature of each zone during VDGS

for tellurium, and only 7.9% of the tellurium was condensed at Levels 2−6 in the condenser.

Under the experimental conditions used in this study, λ was calculated to be 1.52 cm, which was much smaller than the distance between the heating surface and the crucible mouth (L=5.0 cm). The distillation type was viscous distillation because $\lambda < L$ [30]. In contrast to molecular distillation (MD), the tellurium vapor did not readily diffuse out of the crucible mouth. Therefore, as shown in Fig. 4, as the distillation progressed, many tellurium gas molecules accumulated on the evaporation surface and generated a local high pressure. Frequent collision between the evaporating molecules and high internal friction between the gas molecules increased the diffusion resistance of the gas and inhibited the detachment of the molecules from the evaporating surface. In this process, the diffusion of the vaporized metal molecules controlled the entire volatilization process, and most of the tellurium vapor was condensed in Level 1.

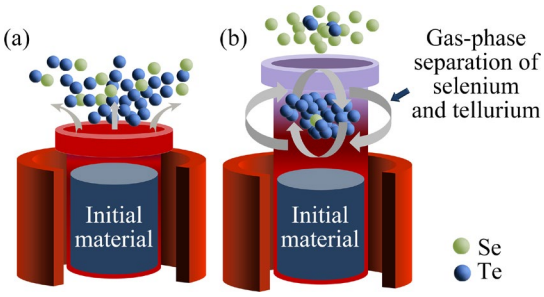

Fig. 4 Diagrams of MD (a) and VDGS (b) systems

Although the evaporation rate of tellurium was reduced, the extent of selenium purification was considerable. Under these experimental conditions, very little selenium condensed at Level 1, the dominant condensation zone for tellurium, which provided gas-phase separation of the selenium and tellurium. As shown in the analysis of the ICP–MS results in Table 1, the selenium volatilized into the gas phase, and most of the selenium was concentrated in the low-temperature condensation zone (Fig. 2(b), Level 6). At Level 1, the selenium content was only 2.59×10^{-4} wt.%. Although the saturated vapor pressure of zinc is similar to that of tellurium, the zinc content in the volatiles was reduced, and most of zinc remained in the crucible because zinc mainly exists in tellurium as ZnTe [32], which has an extremely high melting point (1565 K) and is difficult to volatilize at 723 K.

Therefore, most of zinc remained in the crucible. The ICP–MS results obtained after the VDGS for copper, iron, silicon and other elements with low saturated vapor pressures indicated excellent removal levels, and even the amounts of silicon, iron, bismuth, tin, silver and other elements in the condensation products of each zone were below the detection limit, which was consistent with expectations. As shown in the XRD results in Fig. 5, the sodium impurity in the initial material was mainly Na_2TeO_3, and this remained in the crucible. In addition, there were some TeO_2 and Te in the residue. The volatile matter found in the condensation zones at all levels was pure elemental tellurium. The total impurity content was decreased from 0.190812 wt.% to less than 8.00×10^{-4} wt.%; in other words, the Te in the condensates of Levels 1−4 was purified to higher than 99.9992 wt.%.

Figure 6 shows the SEM images for the Levels 1−6 and condenser cap volatiles and photographs of the initial material and residue. In the Levels 1−6 condensation zones, the morphology of the volatiles was dominated by needle-like crystals. At higher condensation positions, the tellurium vapor density decreased, and the crystal grain sizes decreased. It is worth noting that nanoscale tellurium particles (Fig. 6 (condenser cap)) were obtained from the top plate of the condenser, which may prove to be useful in preparing nanoscale tellurium powder materials.

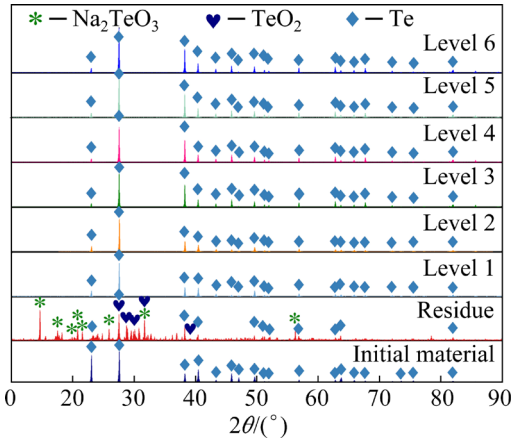

Fig. 5 XRD patterns for initial material, residue, and Levels 1−6 volatiles

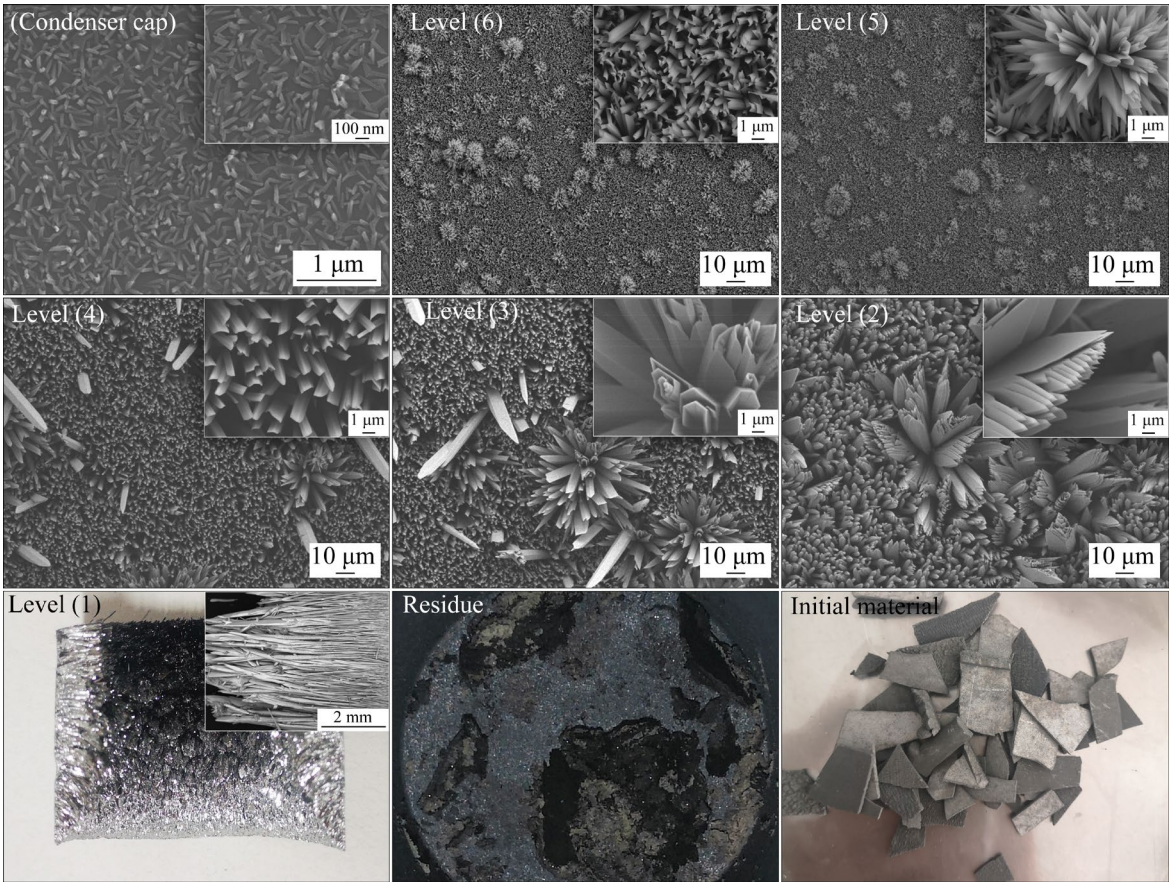

Fig. 6 SEM results for Levels 1−6 and condenser cap volatiles, and photographs of initial material and residue

3.1.2 Effect of distillation temperature and time

To explore the effect of the distillation temperature on the evaporation rate, mass distribution rate for Level 1 and the removal efficiencies for the selenium impurities, the distillation temperature was studied with a distillation time of 120 min and a system pressure of 2 Pa.

As can be seen in Fig. 7(a), with increasing temperature, the evaporation rate increased. When the temperature rose to 773 K, the evaporation rate was greater than 99% and basically remained unchanged with further increase in the temperature. Most of the tellurium condensed at Level 1. However, due to the influence of thermal radiation, the temperature at Level 1 continued to rise with increasing distillation temperature, and the dominant condensation zone for tellurium moved upward, which led to a decline in the mass distribution rate at Level 1. However, an excessively low distillation temperature was not useful for removing selenium. As shown in Table 2, the selenium content at Level 1 was too high at low distillation temperatures and decreased with increasing distillation temperature. Based on the evaporation rate, selenium removal effect, and mass distribution rate at Level 1, 773 K was determined to be the optimal distillation temperature, and the selenium content was reduced to 2.46×10^{-4} wt.%.

The effect of distillation time was studied at a distillation temperature of 773 K and a system pressure of 2 Pa. As shown in Fig. 7(b), with longer distillation time, the evaporation rate continuously increased. After 30 min, the evaporation rate remained basically unchanged. For the Level 1 volatiles, the mass distribution rate decreased slightly with longer time, which may be due to secondary volatilization of the tellurium in the high-temperature condensation zone. As shown in Table 3, selenium was effectively removed from the primary volatiles. Based on these results, 30 min was determined to be the optimal distillation time, and at this time 95.87% of the tellurium was condensed at Level 1 and the selenium content was reduced to 2.57×10^{-4} wt.%.

3.2 Results of 500 g large-scale experiment

In this work, the dominant condensing zone of tellurium was controlled with a two-stage vacuum furnace (Fig. 8). During the experiment, the temperature of the LTHZ was set at 600 K based on the results in Section 3.1 and normal-temperature condensing zone (NTCZ) was cooled by a water-cooling system.

Single-factor experiments designed to probe the effect of distillation temperature were carried out at 723, 773, and 823 K. The other experimental conditions were kept as follows: 90 min distillation

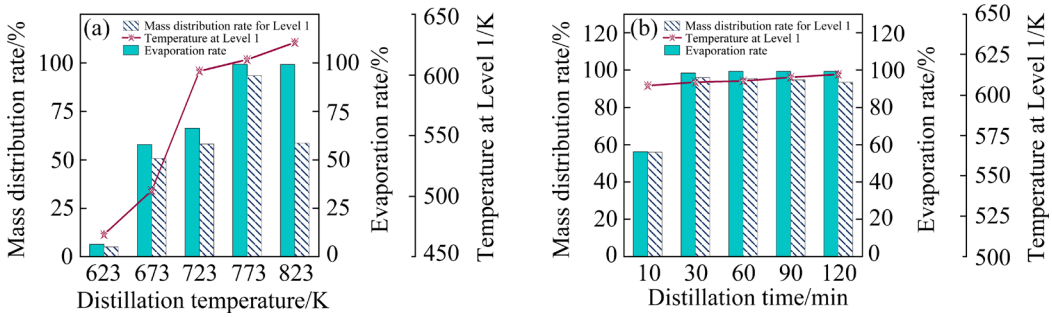

Fig. 7 Effects of distillation temperature (a) and time (b) on mass distribution rate, evaporation rate and temperature at Level 1 during VDGS

Table 2 Selenium contents of Level 1 volatiles produced at different distillation temperatures

Distillation temperature/K	623	673	723	773	823
Content/wt.%	1.387×10^{-3}	9.79×10^{-4}	2.59×10^{-4}	2.46×10^{-4}	2.67×10^{-4}

Table 3 Selenium contents of Level 1 volatiles at different distillation time

Distillation time/min	10	30	60	90	120
Content/wt.%	5.89×10^{-4}	2.57×10^{-4}	2.27×10^{-4}	2.41×10^{-4}	2.67×10^{-4}

time, 5 Pa pressure, and 600 K LTHZ temperature. After the experiment, the condensate in the LTHZ was sampled and analyzed, and the experimental results are shown in Fig. 9(a). With increasing distillation temperature, lead began to volatilize, the lead removal rate decreased and the selenium removal rate did not change significantly, which indicated that high temperatures were not effective in removing lead. When the temperature was increased beyond 773 K, the evaporation rate did not change significantly. Therefore, after considering the evaporation rate, 773 K was identified as the optimum distillation temperature.

As can be shown in Fig. 9(b), single-factor experiments with three distillation time values of 60, 90 and 120 min were carried out at a 5 Pa pressure, a 773 K distillation temperature and a 600 K LTHZ temperature. The removal rates of selenium and lead were basically unchanged as the distillation time was extended, and the evaporation rates did not change significantly after the distillation time was increased beyond 90 min. Based on the energy consumption and efficiency, the optimal experimental conditions involved a distillation temperature of 773 K and a distillation time 90 min. Under the best conditions, the contents of selenium and lead were 2.76×10^{-4} wt.% and 6.70×10^{-5} wt.%, respectively. The removal rates for selenium and lead were 68.28% and 98.64%, respectively, and the contents of the remaining impurity elements were lower than the detection limit of ICP–MS. Ultimately, the direct yield of Te in the LTHZ was 83.40%, and the Te purity reached higher than 99.9996 wt.%.

SEM images and photographs of the residue and condensate produced from a distillation conducted with a pressure of 5 Pa, a temperature of 773 K and a time of 90 min are shown in Fig. 10. The condensate in the LTHZ grew to form needles, which was consistent with results of the small-scale experiments. The black material on the surface of the residue was loose and porous. To determine the

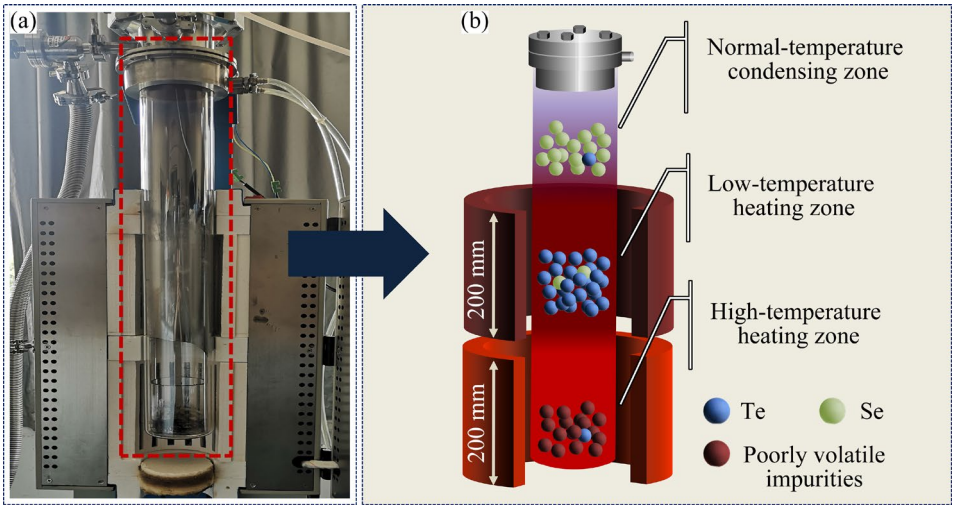

Fig. 8 Photograph (a) and structure diagram (b) of two-stage vacuum furnace

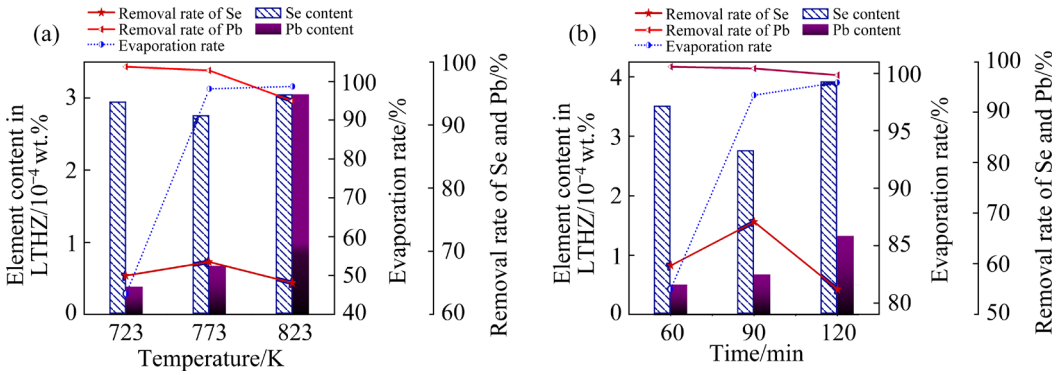

Fig. 9 Effects of distillation temperature (a) and distillation time (b) on content, evaporation rate and removal rate of impurity elements in LTHZ condensate

chemical states of the Te, Cu, Pb, Se and other elements remaining in the residue, EPMA was used to observe the microscale distribution of the impurity elements. Figure 11 shows the EPMA elemental maps of the residue produced at 5 Pa, 773 K and 90 min. The Te was distributed within the plane

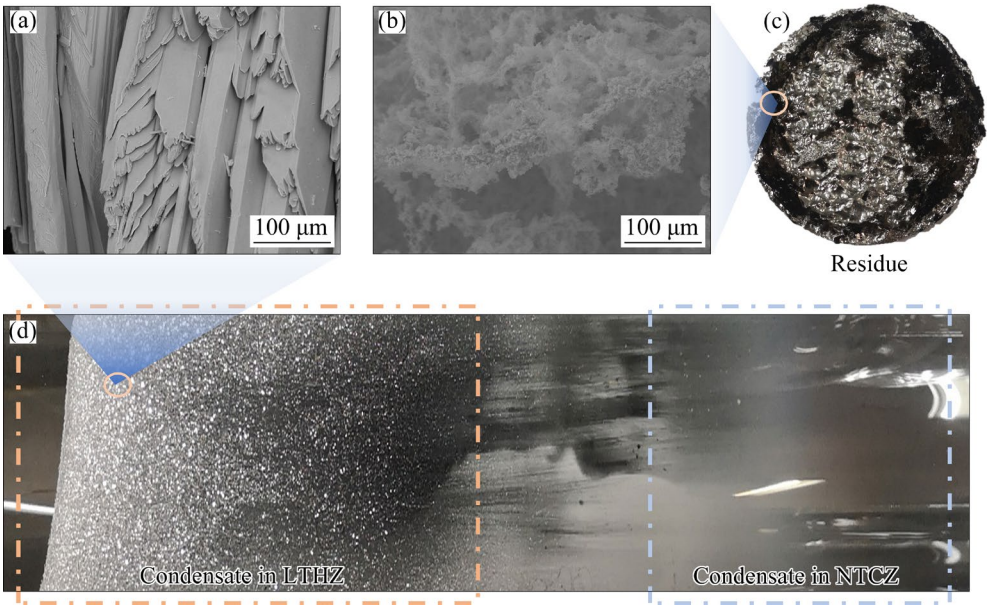

Fig. 10 SEM images (a, b) and photographs of residue (c) and condensates (d) from distillation conducted at 5 Pa, 773 K and 90 min

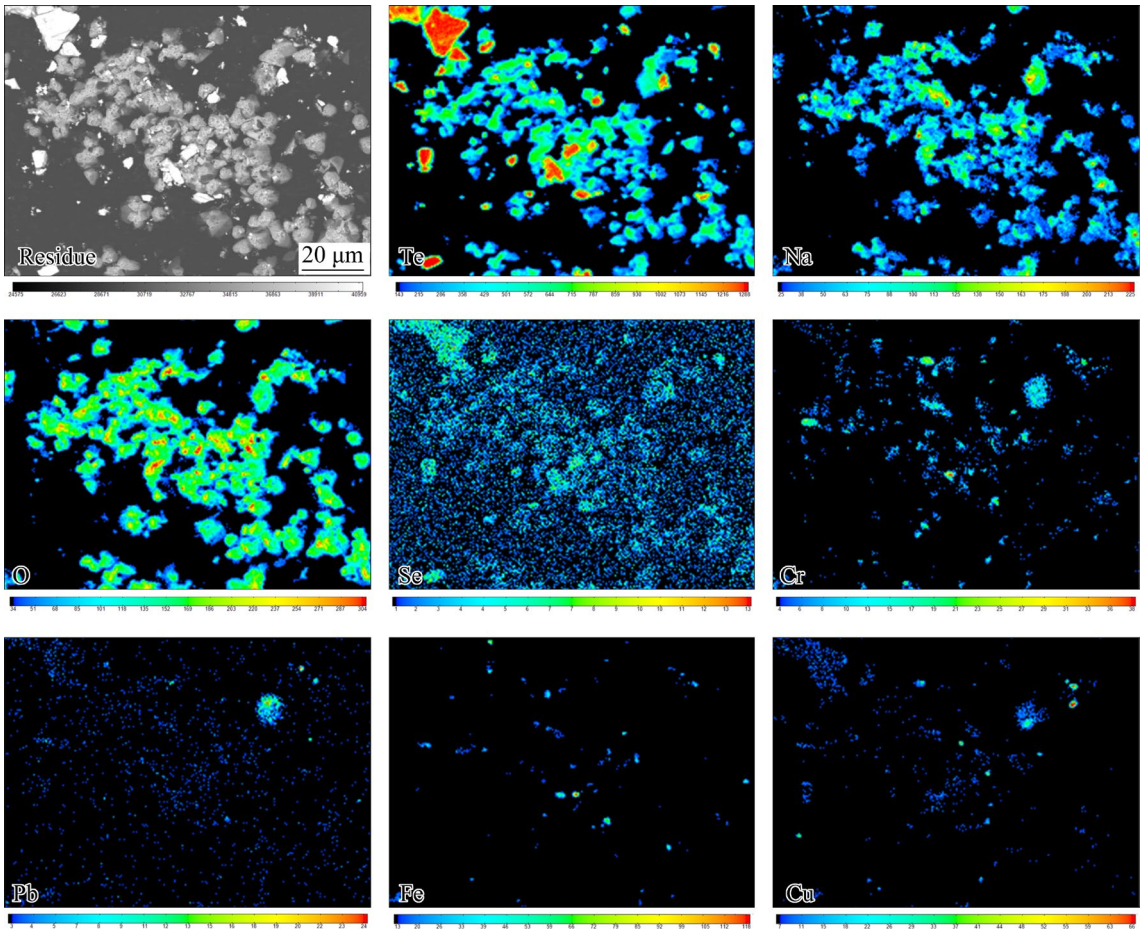

Fig. 11 EPMA elemental maps of residue from distillation conducted at 5 Pa, 773 K and 90 min

scanning range, and it was notably enriched in the brightly colored area, which mainly contained unvolatilized elemental Te. The observations for Na, O and Te confirmed the presence of a Na−Te−O phase, which was consistent with the XRD results. The distributions of Pb, Cu, Se, Cr and other elements were consistent with part of the Te distribution, indicating that the corresponding compounds contained these elements, which hindered Se volatilization and some of the Se remained in the residue.

4 Conclusions

(1) The assessment of the saturated vapor pressure and mean free path of tellurium revealed that the dominant Te condensation zone could be controlled by adjusting the condenser structure and condensing temperature so that poorly volatile substances remained in the crucible, while selenium was separated from the tellurium in the gas phase.

(2) Small-scale experiments showed that the optimum temperature of the Te condensation zone was approximately 600 K. In the dominant condensation zone, Te was purified to higher than 99.9992 wt.%, and the content of Se was reduced from 8.70×10^{-4} wt.% to 2.59×10^{-4} wt.% in the VDGS.

(3) Experiments on the effects of distillation temperature and time showed that an overly low distillation temperature was not useful for separating selenium. Under the optimal experimental conditions (2 Pa system pressure, 773 K distillation temperature and 30 min distillation time), the content of Se was reduced from 8.70×10^{-4} wt.% to 2.57×10^{-4} wt.%.

(4) The optimal experimental conditions for the 500 g upscaled experiment involved a 5 Pa system pressure, a 773 K distillation temperature and a 90 min distillation time. The direct yield of Te in the LTHZ was 83.40%, and the purity of Te reached higher than 99.9996 wt.%.

(5) Waste gas, wastewater and waste residue were not produced in this process. This study also provides a method for separating substances with similar physical properties.

CRediT authorship contribution statement

Da-xin HUANG: Conceptualization, Methodology, Investigation, Writing − Original draft, Writing − Review and editing; **Wen-long JIANG:** Data curation, Project administration, Writing − Review and editing; **Bao-qiang XU:** Project administration, Writing − Review and editing; **Guo-zheng ZHA:** Investigation, Writing − Review and editing; **Bin YANG:** Project administration, Writing − Review and editing.

Declaration of competing interest

The authors declare that they have no known competing financial interests or personal relationships that could have appeared to influence the work reported in this paper.

Acknowledgments

The authors would like to express their sincere thanks to the National Key R&D Program (No. 2022YFC2904900), the National Natural Science Foundation of China (No. U1902221), and the Construction of High-level Talents of Kunming University of Science and Technology, China (No. 20210172), the Leading Talents of Industrial Technology in Ten Thousand Talents Plan of Yunnan Province, China, and the Scientist Studio of Yunnan Province, China.

References

[1] WANG Shi-jie. Tellurium, its resourcefulness and recovery [J]. JOM, 2011, 63(8): 90−93.

[2] BA L A, DÖRING M, JAMIER V, CLAUS J. Tellurium: An element with great biological potency and potential [J]. Organic and Biomolecular Chemistry, 2010, 8(19): 4203−4216.

[3] RAJ A, KUMAR R, CHANDRA R. Thermal analysis of hydrothermally synthesized nanostructured bismuth telluride semiconductor [J]. Materials Today: Proceedings, 2021, 44: 473−481.

[4] WHEIBEL K. The impact of tellurium supply on cadmium telluride photovoltaics [J]. Science, 2010, 328(5979): 699−701.

[5] SONG S. H, WANG J, ISSHIKI M. Preparation and photoluminescence characterization of high-purity CdTe single crystals: purification effect of normal freezing on tellurium and cadmium telluride [J]. Journal of Crystal Growth, 2002, 236(1): 165−170.

[6] KIM W G, LI H, YOO B U, KIM S H, HONG S J, LEE H H, LEE J H. Preparation of Te nanopowder by vacuum distillation [J]. Powder Technology, 2014, 256: 204−209.

[7] LIU Yuan, ZHENG Ya-jie, SUN Zhao-ming. Preparation of high-purity tellurium powder by hydrometallurgical method [J]. Rare Metals, 2014, 33(4): 479−484.

[8] ZHONG Jing, WANG Gang, FAN Jin-long, LI Qing, KIANI M, ZHANG Jie, YANG Hao-wei, CHEN Jin-wei, WANG

Rui-ling. Optimization of process on electrodeposition of 4N tellurium from alkaline leaching solutions [J]. Hydrometallurgy, 2018, 176: 17−25.

[9] GRISHECHKIN M B, MOZHEVITINA E N, KHOMYAKOV A V, ZYKOVA M P, AVETISOV R I, AVETISSOV I K. Deep tellurium purification for the production of electronic and photonic materials [J]. Russian Microelectronics, 2017, 46(8): 551−556.

[10] SUN Zhao-ming, ZHENG Ya-jie. Preparation of high pure tellurium from raw tellurium containing Cu and Se by chemical method [J]. Transactions of Nonferrous Metals Society of China, 2011, 21(3): 665−672.

[11] ZHANG X X, FRIEDRICH S, FRIEDRICH B. Production of high purity metals: A review on zone refining process [J]. Journal of Crystallization Process and Technology, 2018, 8(1): 33−35.

[12] ZAIOUR A, ZAHRAMAN K, ROUMIE M, CHARARA J, FAWAZ A, LMAI F, HAGE-ALI M. Purification of tellurium to nearly 7N purity [J]. Materials Science and Engineering: B, 2006, 131(1/2/3): 54−61.

[13] ABRYUTIN V N, DAVYDOVA E V, EGOROV M A, MARONCHUK I I, SANIKOVICH D D. Profound purification of tellurium, zinc and cadmium for electronic applications [J]. Modern Electronic Materials, 2022, 8(1): 7−14.

[14] LI Zhang-di, QIU Feng-xian, TIAN Qiong, YUE Xue-jie, ZHANG Tao. Production and recovery of tellurium from metallurgical intermediates and electronic waste — A comprehensive review [J]. Journal of Cleaner Production, 2022, 366(15): 132796.

[15] DENG Xue, HUANG Run, LV Xiao-dong, YANG Jing-piao, YANG Jing. Separation and recovery of metallic zinc and iron concentrate from blast furnace dust by vacuum carbothermal reduction [J]. Process Safety and Environmental Protection, 2022, 162: 746−751.

[16] WANG Shuang-ping, ZHAO Jin-yang, XU Bao-qiang, KONG Ling-xin, JIANG Wen-long, YANG Bin. Theoretical research on vacuum separation of Au−Ag alloy [J]. Transactions of Nonferrous Metals Society of China, 2022, 32(8): 2719−2726.

[17] ZHANG Chun-xi, YU Da-wei, GUO Xue-yi, TIAN Qing-hua. Employing magnesium-lead melt for synergetic and selective extraction of copper from copper−cobalt alloy [J]. Transactions of Nonferrous Metals Society of China, 2022, 32(10): 3444−3458.

[18] ZHAN Lu, XU Zhen-ming. Separating and recovering Pb from copper-rich particles of crushed waste printed circuit boards by evaporation and condensation [J]. Environmental Science and Technology, 2011, 45(12): 5359−5365.

[19] CHE Yu-si, MAI Geng-peng, LI Shao-long, HE Ji-lin, SONG Jian-xun, YI Jian-hong. Kinetic mechanism of magnesium production by silicothermic reduction of CaO·MgO in vacuum [J]. Transactions of Nonferrous Metals Society of China, 2020, 30(10): 2812−2822.

[20] ZHA Guo-zheng, YANG Chong-fang, WANG Yun-ke, GUO Xin-yu, JIANG Wen-long, YANG Bin. New vacuum distillation technology for separating and recovering valuable metals from a high value-added waste [J]. Separation and Purification Technology, 2019, 209: 863−869.

[21] YANG Bin, HUANG Da-xin, LIU Da-chun, ZHA Guo-zheng, JIANG Wen-long, KONG Xiang-feng. Research and industrial application of a vacuum separation technique for recovering valuable metals from copper dross [J]. Separation and Purification Technology, 2020, 236: 116309.

[22] PRASAD D S, MUNIRATHNAM N R, RAO J V, PRAKASH T L. Purification of tellurium up to 5N by vacuum distillation [J]. Materials Letters, 2005, 59(16): 2035−2038.

[23] ALI S, PRASAD D, MUNIRATHNAM N, PRAKASH T. Purification of tellurium by single-run multiple vacuum distillation technique [J]. Separation and Purification Technology, 2005, 43(3): 263−267.

[24] MAHMOUDI A, SHAKIBANIA S, MOKMELI M, RASHCHI F. Tellurium, from copper anode slime to high purity product: A review paper [J]. Metallurgical and Materials Transactions B, 2020, 51(6): 2555−2575.

[25] LI H, KIM W G, YOO B W, PARK K T, LEE H H, CHOI J C, HONG S J, KONG M S, LEE H, LEE J H. Numerical analysis and experimental validation of distillation process for purification of tellurium [J]. Separation Science and Technology, 2014, 49(2): 197−208.

[26] GHOSH G, SHARMA R C, LI D T, CHANG Y A. The Se−Te (selenium−tellurium) system [J]. Journal of Phase Equilibria, 1994, 15(2): 213−224.

[27] VOLODIN V N, TREBUKHOV S A, BURABAEVA N M, NITSENKO A V. Melt–gas phase equilibria and state diagrams of the selenium–tellurium system [J]. Russian Journal of Physical Chemistry A, 2017, 91(5): 800−804.

[28] ZHA Guo-zheng, WANG Yun-ke, CHENG Min-qiang, HUANG Da-xin, JIANG Wen-long, XU Bao-qiang, YANG Bin. Purification of crude selenium by vacuum distillation and analysis [J]. Journal of Materials Research and Technology, 2020, 9(3): 2926−2933.

[29] MOHAMED S R, FRIEDRICH S, FRIEDRICH B. Refining principles and technical methodologies to produce ultra-pure magnesium for high-tech applications [J]. Metals, 2019, 9(1): 85.

[30] ZHANG Zhi-qi, WANG Zhi-qiang, CHEN De-hong, MIAO Rui-ying, ZHU Qiong, ZHANG Xiao-wei, ZHOU Lin, LI Zong-an. Purification of praseodymium to 4N purity [J]. Vacuum, 2014, 102: 67−71.

[31] LIANG Ying-jiao, CHE Yin-chang. Inorganic substances thermodynamic data handbook [M]. Shenyang: Northeastern University Press, 1994: 634. (in Chinese)

[32] GUO Yan-ming, GU Yong-ming. Purification of tellurium by vacuum distillation method [J]. Journal of Shanghai University (Natural Science Edition), 1998, 4(3): 264−268. (in Chinese)

基于黏性蒸馏–气相分离的冶金级粗碲提纯方法

黄大鑫[1,2,3]，蒋文龙[1,2,3]，徐宝强[1,2,3]，查国正[1,2,3]，杨 斌[1,2,3]

1. 昆明理工大学 真空冶金国家工程研究中心，昆明 650093；
2. 昆明理工大学 省部共建复杂有色金属资源清洁利用国家重点实验室，昆明 650093；
3. 昆明理工大学 冶金与能源工程学院，昆明 650093

摘 要：开发一种基于黏性蒸馏–气相分离的高纯碲材料制备方法。通过调节冷凝器结构和冷凝温度，达到黏性蒸馏、控制碲优势冷凝区的目的，使挥发性差的物质留在残留物中，而硒在气相中与碲分离，实现冶金级粗碲的提纯。研究饱和蒸气压、碲分子平均自由程、不同冷凝位置的杂质分布特征以及冷凝物形貌。500 g 级的实验结果表明，在 5 Pa、773 K 和 90 min 的最佳实验条件下，碲的直收率为 83.40%，纯度高于 99.9996%，碲优势冷凝区冷凝物中硒含量降低至 2.76×10^{-4}% (质量分数)。

关键词：高纯碲；除硒；提纯；平均自由程；优势冷凝区

(Edited by Wei-ping CHEN)